

Comparative Study of NO and CO Oxidation Reactions on Single-Atom Catalysts Anchored Graphene-like Monolayer

Yanan Tang^{+, * [a, b]}, Weiguang Chen^{+, [a]}, Gao Zhao,^[a] Da Teng,^[a] Yingqi Cui,^[a] Zhaoan Li,^[a] Zhen Feng,^[b] and Xianqi Dai^{*, [b]}

Noble metal single-atom catalysts (NM-SACs) anchored at novel graphene-like supports has attracted enormous interests. Gas sensitivity, catalytic activity, and *d*-band centers of single NM (Pt and Pd) atoms at graphenylene (graphenylene-NM) are investigated using first-principle calculations. The adsorption geometries of gas reactants on graphenylene-NM sheets are analyzed. It is found that the adsorption energies of reactant species on graphenylene-Pt are larger than those on graphenylene-Pd, because the *d*-band center of the Pt atom is closer to the Fermi level. The NO and CO oxidation reactions on graphenylene-NM are investigated via four catalytic mecha-

nisms, including Langmuir-Hinshelwood (LH), Eley-Rideal (ER), New ER (NER), and termolecular ER (TER). The results show that the NO and CO oxidations via LH and TER mechanisms can occur owing to the relatively small energy barriers. Moreover, the interaction of 2NO + 2CO via ER mechanism is the energetically more favorable reaction. Although the NO oxidation via the NER mechanism has rather low energy barriers, the reaction is unlikely to occur due to the low adsorption energy of O₂ compared with CO and NO. This research may provide guidance for exploring the catalytic performance of SACs on graphene-like materials to remove toxic gas molecules.

1. Introduction

Past decades, the rapid development of nanocatalysis and nanoscience play a vital role in the field of chemistry, since the catalysis is the most economical, rational and energy saving approach to achieve energy conversion.^[1] The chemical synthesis of nanocatalysis can provide a platform to study the relationship between surface structure and catalytic activity, and the high density of active sites have well-defined local coordination structure to fabricate appreciable catalytic activity.^[2] Some noble metals (such as Pt, Au)^[3–5] and transition metal oxides^[6–8] have been considered as efficient catalysts in energy storage and industrial production. CO oxidation is often used as a model system to understand catalysis due to its simplicity.^[9] Meanwhile, CO is a toxic gas and harmful to the human health, it is necessary to reduce CO emission from vehicles and industries.^[10] Some works reported that noble metal Pt nanoclusters supported on carbon-based materials (CNTs, carbon black, graphene) can be used as catalysts for CO oxidation.^[11–14] Due to the high cost and high reaction temperature for noble metal (NM) catalysts, it is highly desirable for

maximizing the utilization efficiency of NM atoms by single-atom catalysts (SACs) on supports.^[15] Recent studies have been investigated that metal oxide (such as CeO₂, Fe₂O₃ and Al₂O₃) supported NM-SACs have been used in the heterogeneous catalytic application, e.g., CO oxidation.^[16]


Graphene has received enormous interest due to its two-dimensional (2D) structure, excellence electrical, thermal, optical and mechanical properties.^[17] Noting that pristine graphene is chemically inert and is not active for heterogeneous catalysis,^[18] thus the surface modifications with heteroatoms and creating defects as the efficient strategies to enhance the surface active.^[19–21] Similar as the graphene, graphenylene as a novel *sp*²-hybridized carbon network is composed of hexagonal units (C₆ rings) and square units (C₄ rings)^[22] and has periodic pores with a diameter of 3.2 Å. At present, some theoretical works reported that alkali or alkaline earth metals modified graphenylene supports are considered as high capacity materials for hydrogen and lithium storage.^[23,24] Zhao *et al.* found that the high-efficiency helium separation can be achieved in the inorganic graphenylene from natural gas molecules.^[25] To the best of our knowledge, the graphenylene supported NM-SACs (graphenylene-NM) configurations are rarely discussed, including their structural properties, distribution of active sites and potential applications.

Generally, the catalytic reaction takes place on the surface or interfaces of catalysts, where some gas reactants are adsorbed and then converted into products.^[26] The structure-activity relationships about the underlying gas sensing and catalytic properties for toxic gases on graphenylene-NM are necessary to analyze, such as the influence of stability, geometric and electronic properties of SACs modulated by supported substrate on catalytic activity and selectivity. Hence, it is indispensable to investigate the adsorption stability of NM-SACs on graphenylene sheet as active sites and their related

[a] Dr. Y. Tang,⁺ Dr. W. Chen,⁺ Dr. G. Zhao, Dr. D. Teng, Dr. Y. Cui, Dr. Z. Li
Quantum Materials Research Center
College of Physics and Electronic Engineering
Zhengzhou Normal University, Zhengzhou 450044, China
E-mail: yntang2010@163.com

[b] Dr. Y. Tang,⁺ Dr. Z. Feng, Prof. X. Dai
School of Physics
Henan Normal University
Xinxiang, Henan 453007, China
E-mail: xqdai@zznu.edu.cn

[⁺] These authors contributed equally to this work

 Supporting information for this article is available on the WWW under <https://doi.org/10.1002/cphc.202001021>

 An invited contribution to a Special Collection on Single-Atom Catalysis

electronic structure and magnetic property of systems with gas reactants for much broader catalytic applications. Similar as CO molecule, nitrogen oxides (NO_x) as a typical air pollution are emitted from power plants and off-road equipment,^[27] especially NO is an important insoluble pollutants in flue gas.^[28] The abatement of NO by using strong oxidants to convert NO_2 and then reduced to nitrogen with reductant.^[29] Theoretical study investigated that NO oxidation is feasible on single-atom Pt anchored Al_2O_3 support through the Langmuir-Hinshelwood (LH) pathway.^[30] Although many mechanisms for CO oxidation have been investigated by both experimental and theoretical studies,^[31–33] yet the related reaction mechanisms for NO oxidation are need to further explore and the fundamental issues remaining to be solved, if the CO, NO and O_2 as the flue gases exist at the same time.

Herein, we choose the typical NM catalysts (Pt and Pd) as the candidate to fabricate the configurations of graphenylene-NM and to explore the modulation effects of novel graphene-like material on the catalytic activity of single-atom NM. (1) Is it the catalytic activity of graphenylene-NM sheet is higher than that of the corresponding graphene-NM for CO or NO oxidation? (2) If the answer is yes, which reaction mechanism is the energetically more favorable? In order to answer these questions, we systemically investigate the adsorption behaviors of different gas reactants (including single and double gas molecules) on graphenylene-NM sheets and the possible pathways for CO and NO oxidations have been comparably analyzed through different kinds of reaction mechanisms including LH, Eley-Rideal (ER), New ER (NER) and termolecular ER (TER). Our studies will present the geometries, electronic, gas sensing and catalytic

properties of graphenylene-NM supports, which is beneficial for the design of novel carbon-based material supported NM-SACs with high activity and selectivity.

Computational Details

Spin-polarized density functional theoretical (DFT) calculations are performed using the Vienna *ab initio* simulation package (VASP).^[34,35] The Perdew, Burke, and Ernzerhof (PBE) functional and projector augmented wave (PAW) methods were employed to describe the geometric and electronic properties.^[36,37] The kinetic energy cutoff for the plane-wave basis set is chosen to be 450 eV. The optimized structure of graphenylene in a 2×2 supercell is shown in Figure 1a, and the lattice parameters of graphenylene are $a=b=6.76 \text{ \AA}$.^[22] The vacuum spacing between adjacent layers is 20 \AA . To obtain more accurate electronic structure, the convergence criterion is 10^{-5} eV and the K-points is set to be $3 \times 3 \times 1$ for optimized geometries, as well as $9 \times 9 \times 1$ for density of states (DOS) calculations.

Bader charge analysis^[38] is used to calculate the transferred charges between gas reactants and graphenylene-NM sheets. The minimum-energy pathway (MEP) for elementary reaction step is computed using the climbing image nudged elastic band (CI-NEB)^[39–41] methods. Herein, the spring force between adjacent images is set to be 5.0 eV \AA^{-1} and the force acting on the atoms is chosen as 0.02 eV/\AA . Six images are constructed along the catalytic reaction processes, including the initial state (IS), transition state (TS), intermediate state (MS) and final state (FS).

The adsorption energy (E_{ads}) is defined as [Eq. (1)]:

$$E_{\text{ads}} = E_{\text{A}} + E_{\text{B}} - E_{\text{AB}} \quad (1)$$

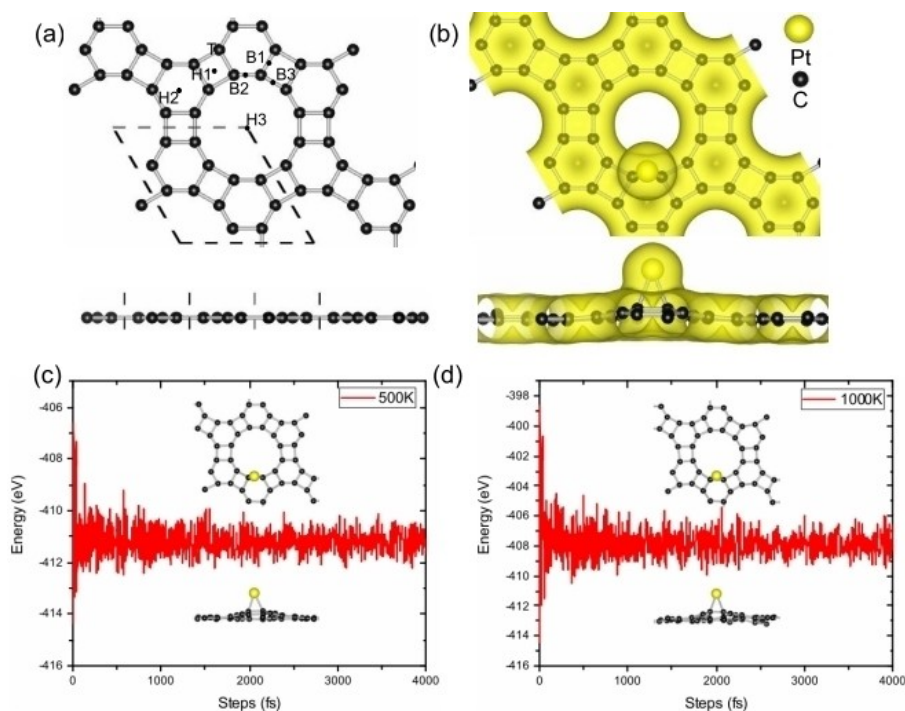


Figure 1. a) The optimized structure of graphenylene. b) Charge distribution (isosurface value is 0.02 e/\AA^3), and molecular dynamics simulation at 500 K (c) and 1000 K (d) for graphenylene-Pt sheets.

where E_A , E_B and E_{AB} are the total energies for gas reactants (A: Pt, Pd, O_2 , O, NO, CO, CO_2 , NO_2 , 2CO, 2NO, O_2 -NO and O_2 -CO), the reactive substrates (B: graphenylene and graphenylene-NM) and the adsorbed systems, respectively.

2. Results and Discussion

2.1. Adsorption Properties of Gas Reactants

Firstly, the quite stable geometries for isolated metal adatoms on graphenylene surface are explored, the single Pt and Pd atoms are anchored at different adsorption sites, which include the hollow site of C–C rings (H1, H2 and H3), the top site of C atom (T) and the bridge site of the C–C bonds (B1, B2 and B3), as seen in Figure 1a. The adsorption energies (E_{ads}) for Pt and Pd atoms at different sites are listed in Table 1, this result shows that the Pt and Pd adatoms at the B3 site (2.50 eV and 1.51 eV) are more stable than that on others sites (B, T and H) and the calculated bond lengths between metal and carbon atoms are about 2.04 Å and 2.12 Å, respectively. Secondly, the valence charge distributions of graphenylene-Pt system are shown in Figure 1b, where the isosurface value is 0.02 e/Å³. It is clearly seen that the more electrons are accumulated at the C–Pt–C interfaces, illustrating that the transferred electrons (0.13 e) between Pt atom and graphenylene can promote the stability of anchored catalyst. As a reference, the single-atom Pt and Pd supported at B site of pristine graphene are also considered (1.55 eV and 1.07 eV),^[42] the relatively large E_{ads} of metal adatoms indicate that the graphenylene substrate can enhance the stability of supported metal adatom. Hence, the single Pt and Pd atoms prefer to anchor at the B3 site and exhibit the more stability than those on graphene surface.

In order to check the thermodynamics stability of graphenylene-NM configurations, we use the first principles molecule dynamics (FPMD) calculations to investigate the thermal stability of graphenylene-Pt sheet, as shown in Figure 1c–d. In MD simulations the structural parameters a, b, and c are allowed to change. A time step of 1.0 fs is used and the temperature is controlled by velocity scaling at each step. The total 4000-time steps (4000 fs) are performed for each MD run and the temperature was set at 500 K and 1000 K. In a period of 4000 fs (4 ps), it is clearly shown that the anchored Pt atom on graphenylene plane has slight distortion, yet the formation geometries of graphenylene-Pt configurations still exhibit highly stability.

Based on the stable configurations of graphenylene-NM substrates, the adsorption geometries of single gas molecules (CO, NO, O_2 , O, CO_2 , NO_2) on graphenylene-Pt and graphenylene-Pd surfaces are investigated, the corresponding energies

and structural parameters for these optimized configurations are shown in Table 2. The end-on configurations for single NO and CO are anchored at graphenylene-Pt sheet, as shown in Figures 2a–b, the adsorbed NO has relatively larger E_{ads} (2.36 eV) than that of CO molecule (2.25 eV) and the Pt–NO distance is 1.80 Å, which is smaller than that of the CO–Pt distance (1.85 Å). As shown in Figure 2c, the O–O bond of O_2 is parallel to the graphenylene-Pt and forms two Pt–O bonds with an E_{ads} of 1.07 eV, and the Pt– O_2 distance is about 2.03 Å. Compared to graphene-Pt sheet (CO, 2.84 eV and O_2 , 1.39 eV),^[43] the anchored gas reactants have smaller E_{ads} on graphenylene-Pt. Among these adsorbed gases (CO, NO and O_2), the single O atom exhibits the more stability with an E_{ads} of 4.20 eV and the Pt–O distance is 1.77 Å, as seen in Figure 2d. In addition, the adsorbed CO_2 and NO_2 molecules have large energy difference (1.36 eV), and the Pt– CO_2 and Pt– NO_2 distances are about 2.16 Å and 2.00 Å, as seen in Figures 2e–f. These results mean that the generation of CO_2 is more easily desorbed from the surface of catalysts, yet the stability of NO_2 is quite high and so the releasing the produced NO_2 is rather rate-determining.

In order to analyze the electronic and magnetic properties of graphenylene-NM sheets with the adsorption of gas reactants, the valence charge density plots and spin charge distributions for gas reactants adsorbed systems are seen in Figure 3, where the isosurface values are 0.02 e/Å³ and 0.001 e/Å³, respectively. Figures 3a–c show that the valence electrons are mainly accumulated in the vicinity of the NO–Pt, O_2 –Pt and NO_2 –Pt interfaces, illustrating that the existing of more transferred electrons (0.33 e, 0.44 e and 0.47 e) between adsorbates and catalysts and thus promote the stability of gas reactants. Compared with CO molecule (0.22 e), the adsorbed NO gains more transferred electrons (0.33 e) and exhibits the higher stability. In addition, the O_2 as an electron-acceptor molecule easily gain more electrons (0.44 e), resulting in the elongation of the O–O bond (1.33 Å). Furthermore, the adsorbed gases cause the changed magnetic properties of graphenylene-Pt system. Figures 3d–f show that the more number of spin charge are distributed at the O_2 –Pt interfaces, which has larger magnetic moment (1.96 μ_B) than those of the adsorbed NO and

Table 1. The calculated E_{ads} (in eV) of metal atoms at different adsorption sites.

Metal adatom	Adsorption site						
	B1	B2	B3	H1	H2	H3	T
Pt	1.98	1.84	2.50	1.62	–	–	–
Pd	1.34	1.33	1.51	1.34	1.02	–	–

Table 2. The adsorption energies (E_{ads} , in eV), adsorption heights of gas species (d_1 , in Å), bond lengths of C–O, N–O or O–O (d_2 , Å) and the transferred electrons (Δq_{1i} , in e) from Pt (or Pd) atoms to adsorbates. The system states the graphenylene-achored metal and the adsorbed species.

System	E_{ads} [eV]	Δq_{1i} [e]	d_1 [Å]	d_2 [Å]
Pt/CO	2.25	0.22	1.85	1.16
Pt/NO	2.36	0.33	1.80	1.18
Pt/ O_2	1.07	0.44	2.03	1.33
Pt/O	4.20	0.71	1.77	–
Pt/ CO_2	0.06	0.04	2.16	1.18
Pt/ NO_2	1.42	0.47	2.00	1.21–1.34
Pd/CO	1.56	0.16	1.89	1.15
Pd/NO	1.69	0.25	1.86	1.18
Pd/ O_2	0.95	0.37	2.08	1.30
Pd/O	3.36	0.60	1.84	–
Pd/ CO_2	0.02	0.03	2.17	1.17
Pd/ NO_2	1.13	0.46	2.06	1.21–1.30

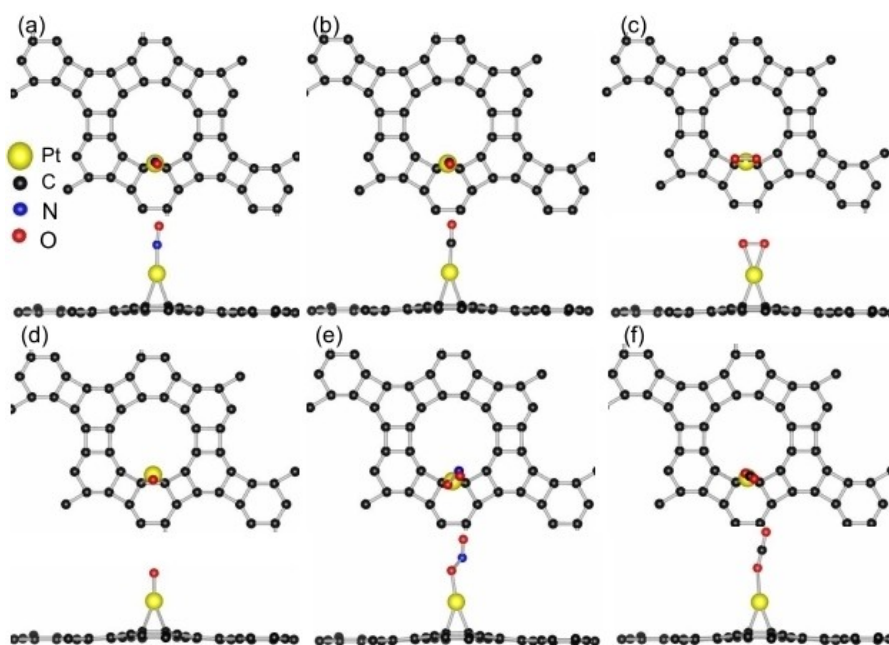


Figure 2. Stable configurations of a) NO, b) CO, c) O₂, d) O, e) NO₂, and f) CO₂ on graphenylene-Pt.

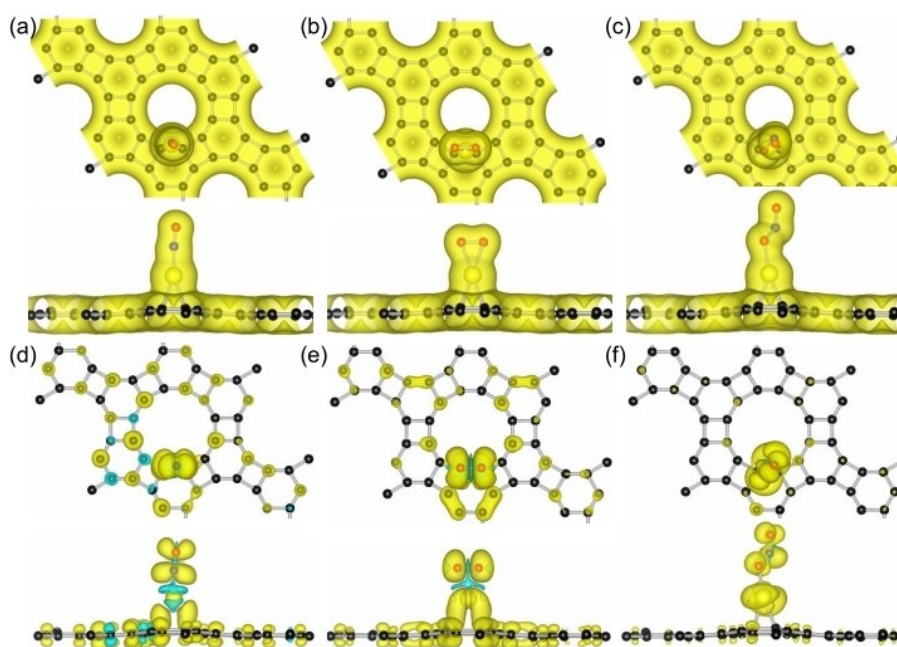


Figure 3. a–c) Charge distribution and d–f) spin charge distribution for NO, O₂ and NO₂ on graphenylene-Pt sheets, where the isosurface values are 0.02 e/Å³ and 0.001 e/Å³, respectively.

NO₂ systems. Compared with the adsorbed NO (1.0 u_B), the less spin electrons are distributed at the graphenylene surface and thus the NO₂ adsorbed system has relatively smaller magnetism (0.85 u_B). Therefore, the different kinds of gas reactants can turn the magnetic properties of graphenylene-Pt systems.

To further study the origin of stability for metal adatoms and adsorbed gas molecules on graphenylene systems, the corresponding DOS plots for adsorbates on substrates are

discussed, as shown in Figure 4. For the graphenylene-NM systems, the symmetry of spin channels in graphenylene system is largely changed after the Pt and Pd atom is adsorbed. For the graphenylene-Pt system, there is a small band gap of 0.2 eV meaning that the Pt adsorbed system is a semiconductor property, and the symmetry of spin channels indicate that it has nonmagnetic property, as seen in Figure 4a. The black solid, red solid and blue solid curves represent the TDOS of graphenylene,

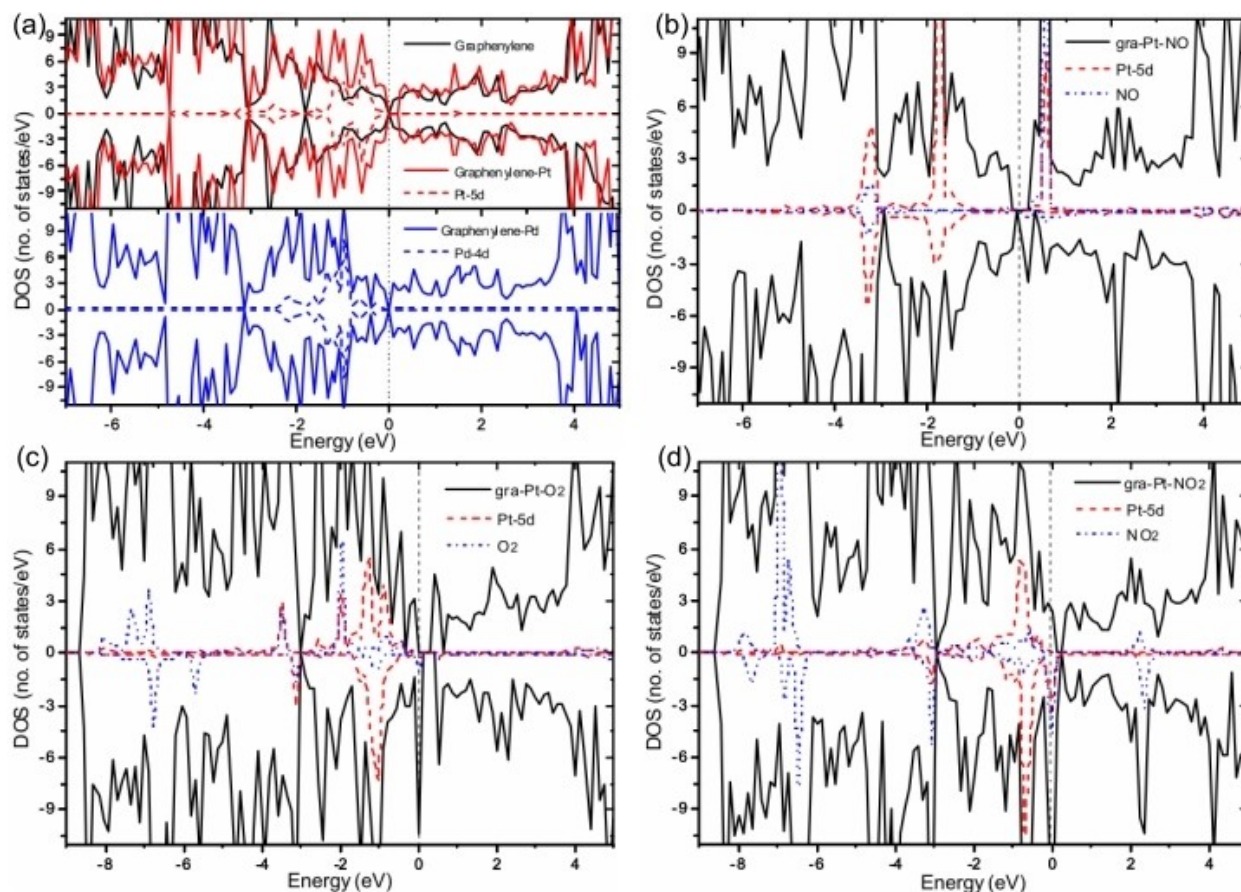


Figure 4. The DOS plots for a) graphenylene-NM systems and b) NO, c) O₂, and d) NO₂ adsorbed on a graphenylene-Pt sheet.

graphenylene-Pt and graphenylene-Pd systems, as well as the red dashed and blue dashed curves represent the PDOS of Pt-5d and Pd-4d orbitals, respectively. It is shown that the PDOS of Pt-5d and Pd-4d orbitals strongly hybridize with the TDOS of graphenylene-M below the Fermi level (E_F), denoting that the *d*-orbital electrons can promote the adsorption stability of metal catalysts, which is in agreement with the previous results.^[44] Besides, the *d*-band center of Pt atom (−1.25 eV) is more close to the Fermi level (E_F) than that of the Pd atom (−1.34 eV). Generally, the closer the *d*-band centers to E_F of metal catalyst, the stronger it binds to adsorbates,^[45,46] thus the supported Pt atom on graphenylene may enhance the adsorption of gas reactants. Table 2 shows that the calculated E_{ads} of reactive gases on graphenylene-NM surface, the adsorptions of NO, CO, O₂ and O on Pt catalysts are more stable than those on Pd atom. Because of these gas reactants gain more transferred electrons (0.33 *e*, 0.22 *e*, 0.44 *e*, 0.71 *e*) from the Pt atoms as compare with those on Pd atoms (0.25 *e*, 0.16 *e*, 0.37 *e*, 0.60 *e*), illustrating that the anchored Pt atom at graphenylene exhibits the higher reactivity.

In Figures 4b–d, the black solid, red dashed and blue dash dotted curves represent the TDOS of gas adsorbed graphenylene-Pt systems, the PDOS of Pt-5d orbitals and the LDOS of adsorbed gases, respectively. Compared with the TDOS of graphenylene-Pt, the adsorptions of NO, O₂ and NO₂ cause the

TDOS redistribution of reactive substrate. The asymmetry of spin channels nearby the E_F indicates that the adsorbed gases systems have magnetic moments (1.0 μ_B , 1.96 μ_B and 0.85 μ_B), which is consistent with the trend of spin charge distributions. In addition, there are strong hybridizations between the broadened Pt 5d states and LDOS of adsorbed gases. There is a band gap in spin-up channels and one DOS peak appears at the E_F in spin-down channels, illustrating the NO adsorbed system is semimetal property. For the O₂ and NO₂ adsorbed systems, the spin DOS peaks appear at the E_F , meaning that the semiconducting property of graphenylene-Pt becomes the metal property. These results illustrate that the different kinds of metal adatoms and gas molecules can effectively turn the magnetic and electronic properties of graphenylene system.

2.2. Coadsorption of Gas Molecules

Different from the single gas molecule, the coadsorption of gas reactants as IS may influence on the reactive mechanisms for NO and CO oxidations. The stable coadsorption configurations of gas molecules (2NO, 2CO, NO–O₂, and CO–O₂) on graphenylene-Pt surface are further explored, as seen in Figure 5, and the calculated E_{ads} and structural information are summarized in Table 3. From Figures 5a–b, the 2NO molecules anchored at Pt

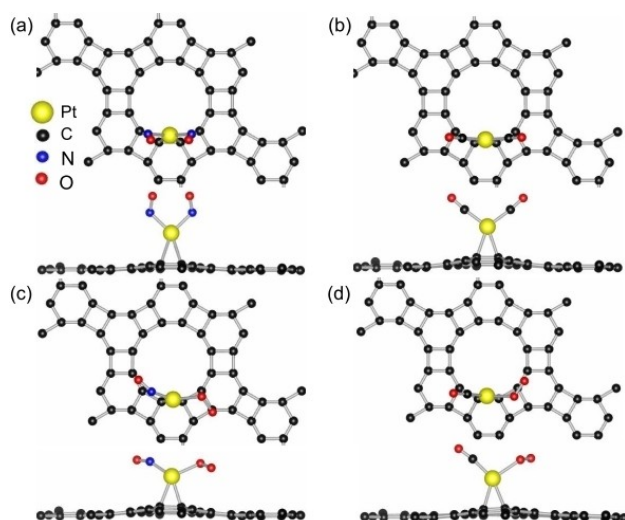


Figure 5. Coadsorption configurations for a) 2NO, b) 2CO, c) NO–O₂, and d) CO–O₂ on a graphenylene-Pt sheet.

Table 3. The coadsorption energies (E_{ads} , in eV), adsorption heights of gas reactants (d_3 , in Å), bond lengths of C–O, N–O or O–O (d_4 , in Å) and the number of transferred electrons (Δq_2 , in e) from Pt (or Pd) atoms to adsorbates. The system states the graphenylene-achored metal and the adsorbed species.

System	E_{ads} [eV]	Δq_2 [e]	d_3 [Å]	d_4 [Å]
Pt/CO–O ₂	2.41	0.18	1.87	1.16
		0.23	2.25	1.26
Pt//NO–O ₂	2.71	0.26	1.83	1.18
		0.44	2.11	1.30
Pt/2CO	3.16	0.13	1.92	1.15
		0.13	1.92	1.15
Pt/2NO	3.22	0.21	1.99	1.19
		0.21	1.99	1.19
Pd/CO–O ₂	1.58	0.15	1.93	1.16
		0.27	2.21	1.26
Pd//NO–O ₂	2.09	0.20	1.88	1.18
		0.40	2.12	1.29
Pd/2CO	2.14	0.14	1.95	1.15
		0.14	1.95	1.15
Pd/2NO	2.61	0.21	1.96	1.19
		0.21	1.96	1.19

atom has the relatively larger E_{ads} (3.22 eV) than that of 2CO (3.16 eV), and the distances between 2NO and Pt atom (1.99 Å) are larger than that of the CO–Pt distances (1.92 Å). Besides, the coadsorbed NO–O₂ (2.71 eV) molecules on graphenylene-Pt sheet are more stable than those of the CO–O₂ (2.41 eV), and these coadsorbed gases are more stable than the isolated ones. These results indicate that the coadsorption of gas molecules tend to anchor at the active site of Pt atom if an O₂, NO and CO mixture as the fuel gases. Compared with graphenylene-Pt sheet, the coadsorptions of gas molecules on graphenylene-Pd have relatively smaller E_{ads} (2.61 eV for 2NO, 2.14 eV for 2CO, 2.09 eV for NO–O₂ and 1.58 eV for CO–O₂), and the larger energy difference between NO–O₂ and CO–O₂ indicating that the supported Pd on graphenylene may exhibits less gas sensitivity.

As shown in Figures 6a–b, the coadsorptions of gas molecules induce the valence charge redistributions of graphenylene-Pt system, where the isosurface value is 0.003 e/Å³. It is clearly shown that the more electrons are accumulated at NO–Pt–O₂ and CO–Pt–O₂ interfaces than those on graphenylene support. Compared with NO (0.26 e) or CO (0.18 e) molecule, the coadsorbed O₂ gains more transferred electrons (0.44 e, 0.23 e) from the supported Pt catalysts. Meanwhile, these coadsorbed gas reactants also modulate the spin electrons redistributions of graphenylene-Pt system, where the isosurface value is 0.001 e/Å³, as seen in Figures 6c–d. The more number of spin electrons are distributed at CO–Pt–O₂ interfaces than those of NO–Pt–O₂ system, so the coadsorbed CO–O₂ on system has larger magnetic moment (2.0 μ_B). Furthermore, the spin up electrons is accumulated at O₂ molecule than those of CO and NO adsorption. Therefore, the different kinds and number of gas molecules can effectively turn the change of magnetic property of supported substrate.

2.3. Reaction Mechanisms

The calculated results show that the isolated or coadsorbed gas reactants on graphenylene-Pt are more stable than those on graphenylene-Pd sheet. The coadsorptions of gas molecules have larger E_{ads} than that of isolated ones, thus these reactive species (CO–O₂, NO–O₂, 2NO and 2CO) on graphenylene-Pt sheet as the IS configuration would be considered for NO and CO oxidations. For the LH mechanism, the interaction between O₂ and CO (or NO) directly form a peroxo-type OOCO (or OONO) complex and the dissociation reactions for OOCO (or OONO) to form the product of CO₂ or NO₂.^[47–50] In the mixture of NO and CO flue gas, the coadsorbed 2NO at NM-SACs are more stable than that of 2CO molecules, thus the preadsorbed NO molecules prefer to occupy the active site and to proceed

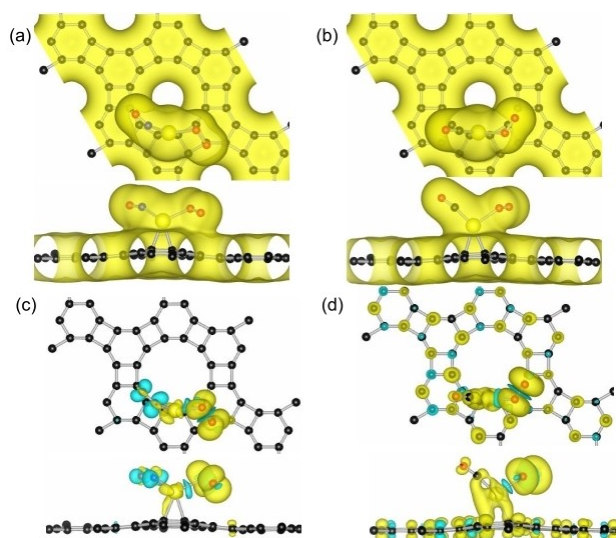


Figure 6. a–b) Charge distribution and c–d) spin charge distribution for NO–O₂ and CO–O₂ on graphenylene-Pt, where the isosurface values are 0.003 e/Å³ and 0.001 e/Å³, respectively.

the CO oxidation via ER mechanism.^[51] In addition, the preadsorbed 2CO or 2NO may be directly oxidized by one O₂ molecule, which as a possible termolecular ER (TER) mechanism has been considered.^[52]

2.3.1. LH Mechanism

For the LH mechanism, the catalytic reactions for NO and CO oxidations are comparably investigated in Figure 7. At the IS configuration, the coadsorption of NO* and O₂* are tilted at Pt catalyst, where the NO–O₂ distance is about 3.40 Å. From the IS to MS1, the O atom of O₂ turns around and approaches to the N atom of NO to reach the TS1, which need to overcome the energy barrier (*E*_{bar}) of 0.22 eV and the NO–O₂ distance is shorted to 2.51 Å, as seen in Figure 7a. Passing over TS2, the OONO* complex is generated at the Pt catalyst with an *E*_{bar} of 0.34 eV and the O–O bond is elongated to 1.39 Å. To process, the O–O bond of OONO* complex is dissociated from 1.39 Å to 3.56 Å, this reaction via the TS3 has an *E*_{bar} of 0.17 eV, resulting in the O–O bond is broken and then one NO₂ is generated, leaving an O atom anchors at Pt catalyst (FS). For the coadsorbed CO* and O₂* molecules on graphenylene-Pt sheet, the corresponding reaction processes through TS1, TS2 and TS3

are displayed in Figure 7b. From IS to MS2, the OOCO* complex is formed with the relatively larger *E*_{bar} (0.27 eV and 0.36 eV) than that of the OONO* complex, while the dissociated reaction to generate CO₂ molecule and one O atom without any energy barrier. The formed CO₂ with much small *E*_{ads} (0.06 eV and 0.02 eV) are desorbed easily from Pt and Pt catalysts. As shown in Figure S1 in the Supporting Information, the second CO oxidation occurring with the remaining O atom through LH mechanism is also investigated, and the corresponding *E*_{bar} is about 0.22 eV and 0.25 eV. For LH mechanism reactions, the rate-controlling step in the first CO oxidation has relatively large *E*_{bar} (0.36 eV).

Furthermore, the NO and CO oxidation processes through LH mechanism on graphenylene-Pd sheet are investigated and the corresponding *E*_{bar} are summarized in Table 4. Compared with graphenylene-Pt sheet (0.34 eV), the interaction between NO and O₂ molecules on graphenylene-Pd to generate the OONO complex with the smaller *E*_{bar} (0.31 eV). In the NO oxidation processes, the LH reactions through TS2 (NO* + O₂* → OONO*) is viewed as the rate-controlling step. Different from the releasing CO₂ product, the formation of NO₂ molecule and leaving O atom tends to anchor at the graphenylene-NM surfaces, and the corresponding oxidation reactions for O atom reacting with second NO molecule through ER mechanism are

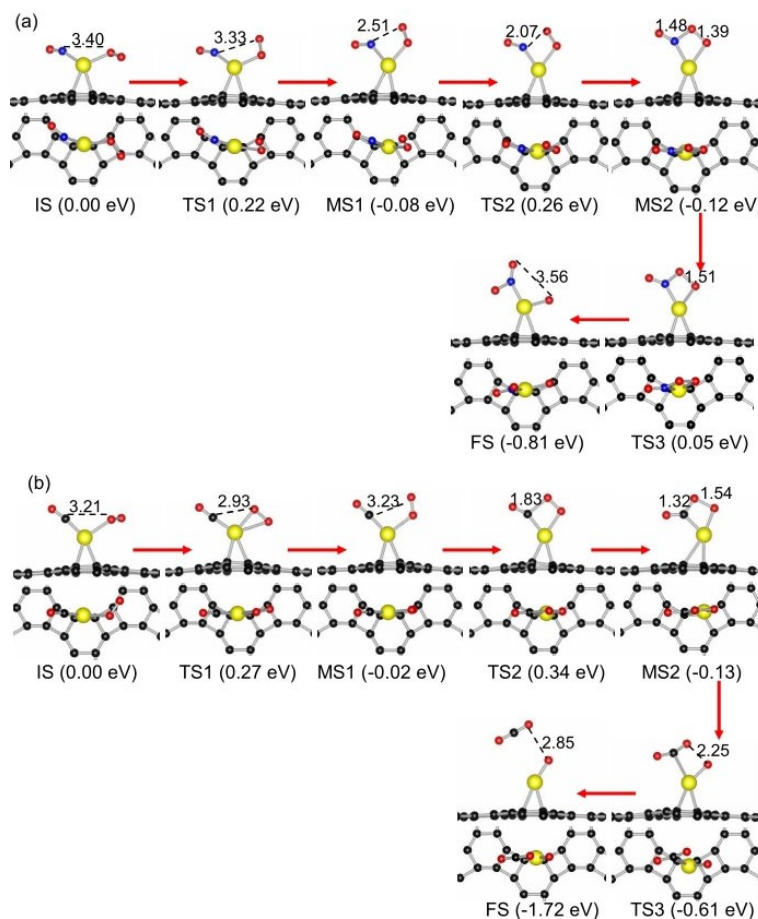


Figure 7. Reaction pathways for a) NO oxidation and b) CO oxidation through LH mechanism.

Table 4. The calculated energy barriers (E_{bar} in eV) for NO and CO oxidation on graphenylene-NM sheets.

Reaction substrates	Reaction mechanisms LH ($E_{\text{bar}1}$, $E_{\text{bar}2}$, $E_{\text{bar}3}$) NO + O ₂ → OONO → NO ₂ + O CO + O ₂ → OOCO → CO ₂ + O	ER ($E_{\text{bar}4}$) O + NO → NO ₂ O + CO → CO ₂	ER ($E_{\text{bar}5}$, $E_{\text{bar}6}$) 2NO + 2CO → 2CO ₂ 2 N → N ₂ ($E_{\text{bar}7}$)	TER ($E_{\text{bar}8}$, $E_{\text{bar}9}$) 2NO + O ₂ → ONO-ONO → 2NO ₂ 2CO + O ₂ → OCO-OCO → 2CO ₂ NER ($E_{\text{bar}10}$, $E_{\text{bar}11}$) O ₂ + 2NO → OONNOO → 2NO ₂ O ₂ + 2CO → OOCOCO → 2CO ₂
graphenylene-Pt	0.22, 0.34, 0.17 0.27, 0.36, 0.00	0.00, 0.12,	0.27, 0.21, 0.07	0.11, 0.38, 0.74, 0.61 0.18, 0.00, 0.81, 0.64
graphenylene-Pd	0.29, 0.31, 0.04 0.30, 0.33, 0.00	0.00, 0.05,	0.35, 0.30, 0.00	0.00, 0.33, 0.73, 0.48 0.14, 0.00, 0.07, 0.00

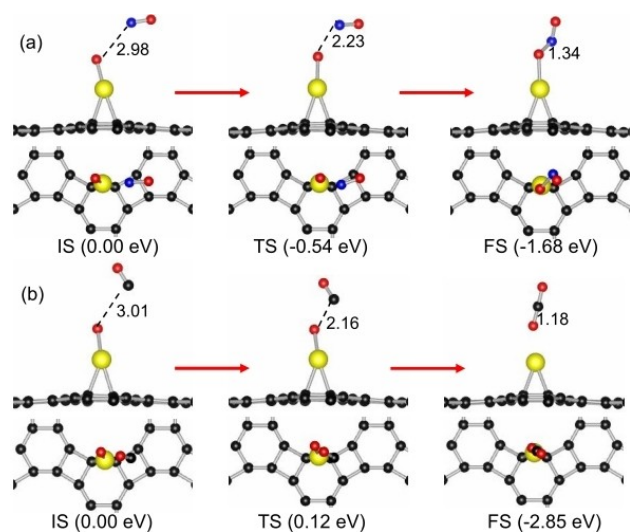
investigated, as shown in Figure S2. The NEB calculation results show that the formations of second NO₂ molecules are barrierless process with endothermic energies of −2.04 eV and −2.44 eV, respectively. Then, the single NO and CO oxidation reactions (NO or CO + O* → NO₂* or CO₂*) to generate the one NO₂ or CO₂ molecule via ER mechanism are studied in Figure 8, and the calculated E_{bar} are summarized in Table 4.

Compared with the coadsorbed reactants through LH mechanism, the formation of second NO₂ and CO₂ molecules via ER mechanism on graphenylene-Pt has smaller energy barriers. In addition, the CO oxidation reaction (CO + O* → CO₂) on graphenylene-Pd has much lower E_{bar} (0.05 eV) due to the anchored O atom at Pd atom has relatively smaller E_{ads} (3.36 eV). Generally, the interaction between the active sites of catalysts and reactive gases should neither be too strong nor too weak.^[46] If the interaction is too strong, the gas reactants have large difficulty in dissociating and then forming products. For the LH mechanism reactions, the graphenylene-Pt (and -Pd) sheets exhibit the higher catalytic activities for NO and CO oxidations (< 0.4 eV) than those on Mn (0.95 eV and 1.24 eV), Ni (0.73 eV and 0.53 eV) and Ru atoms (0.82 eV and 0.67 eV),^[53,54] since the relatively weak coadsorption of gas reactants on Pt and Pd catalysts (< 0.3 eV) as starting step are easier to proceed.

Meanwhile, these CO oxidation reactions on graphenylene-Pt (and -Pd) sheets also have smaller energy barriers than the single-atom doped graphene substrates, such as Cu (0.54 eV),^[55] Pt (0.46 eV),^[56] Pd (0.60 eV),^[57] Fe (0.64 eV).^[47] These results illustrate that different reactive substrates play an important role in turning the adsorption stability and activity of metal catalysts, resulting in affect the catalytic reaction mechanisms and energy barriers.^[58] Therefore, the formations of graphenylene-NM may be an efficient catalysts for NO and CO oxidation.

2.3.2. ER Mechanism

Recent study reported that the possible catalytic reaction between CO and NO molecules [NO + CO → N₂ + CO₂] on Pt nanoclusters at low temperature range,^[32] indicating that the CO and NO both exist at the same time in flue gases. As an important reference, the high stability of NO molecules may promote the oxidation of CO on the surface of graphenylene-NM, and the corresponding reaction pathways [2NO* + 2CO → N₂* + 2CO₂] through ER mechanism on graphenylene-Pt are investigated, as displayed in Figure 9. Firstly, two CO molecules are suspended above the preadsorbed 2NO on Pt catalyst (IS) and the distances between CO and NO are about 3.32 Å. From IS to MS, the first CO₂ is formed through TS1 with an E_{bar} of 0.27 eV. To proceed, another CO is close to the O atom of NO and their distance is decreased from 3.38 Å to 2.82 Å. Finally, the second CO₂ molecule is generated through TS2 (0.21 eV). After the formation of 2CO₂ are desorbed, the leaving two N atoms are adsorbed at Pt catalyst and the formation reaction for N₂ molecule is analyzed in Figure 9b, this process need to overcome an E_{bar} of 0.07 eV. Compared with the LH mechanism, the 2CO molecules more easily react with 2NO to generate 2CO₂ via ER mechanism (< 0.3 eV) and then form one N₂ molecule, so the ER mechanism is an energetically more favorable. Therefore, the interaction of 2NO + 2CO reactions to produce 2CO₂ and N₂ can easily occur and to avoid catalyst CO poisoning. On the graphenylene-Pd sheet, the same ER reactions between 2NO and 2CO are considered and the calculated E_{bar} are listed in Table 4. It is found that the CO oxidation reactions via ER mechanism on graphenylene-Pd have relatively larger E_{bar} (0.35 eV and 0.30 eV), yet the generation of N₂ molecule is a barrierless process. These results illustrate that the CO catalytic oxidation to occur well on graphenylene-NM

**Figure 8.** The reaction pathways for a) NO + O and b) CO + O through ER mechanism.

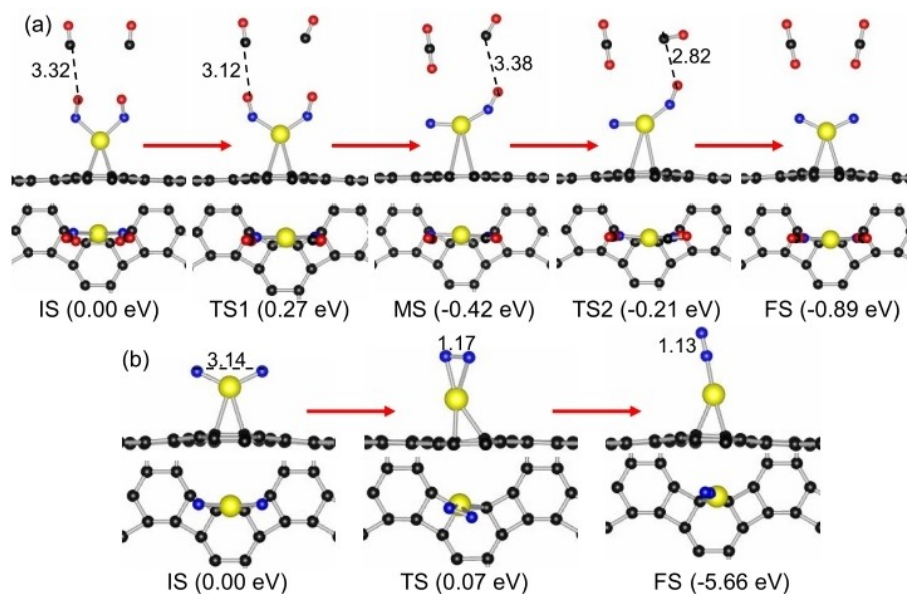


Figure 9. The reaction pathways for a) 2NO–2CO and b) the formation of N₂ molecule.

sheets through ER mechanism under a mixture of NO + CO reaction conditions.

2.3.3. TER Mechanism

Different from the LH and ER mechanisms, the TER as a new reaction mechanism is that the gaseous O₂ molecule is activated by preadsorbed 2NO (or 2CO) molecules at single metal catalyst,^[57] the probably TER pathway follows: 2NO* + O₂ → ONOONO* → 2NO₂ or 2CO* + O₂ → OCOOCO* → 2CO₂. According to the calculated E_{ads}, the single NO and CO molecule

or the coadsorbed 2NO and 2CO are more stable than the adsorbed O₂, thus the coadsorbed 2NO or 2CO easily occupy at the Pt catalyst and start from the coadsorption of NO–Pt–NO or CO–Pt–CO configurations (IS), as displayed in Figure 10, and the corresponding E_{bar} are summarized in Table 4. Figure 10a shows that one O₂ molecule approaches to 2NO molecules and then two oxygen atoms binds to the N atoms of NO molecules (MS). From IS to MS, the O₂–NO distances are decreased from 3.32 Å to 1.70 Å and this reaction has an E_{bar} of 0.11 eV. From MS to FS, the O–O bond is decreased from 1.36 Å to 2.79 Å and the formation of 2NO₂ molecules has a large E_{bar} of 0.38 eV, which is

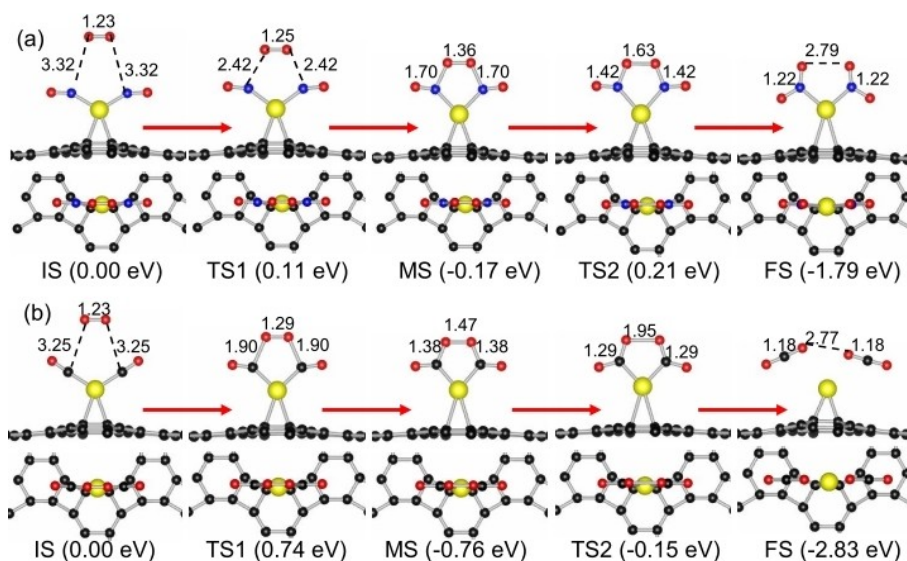


Figure 10. The reaction pathways for a) 2NO–O₂ and b) 2CO–O₂ via the TER mechanism.

relatively difficult to dissociate the ONO–Pt–ONO (MS) as compared with the generation reaction.

Figure 10b shows the CO oxidation reactions on graphenylene-Pt via TER mechanism. From IS to MS, the O₂–CO distances are decreased from 3.25 Å to 1.38 Å and the O–O bond is stretched from 1.23 Å to 1.47 Å. The generation of OCO–Pt–OCO pentagonal ring has larger E_{bar} (0.74 eV) than the formation of ONO–Pt–ONO configuration. To proceed, the dissociation of OCO–Pt–OCO ring to generate 2CO₂ with a relatively small E_{bar} of 0.61 eV and the formed CO₂ would be released. Compared with the interaction of 2CO and O₂ via TER reactions (>0.60 eV), the formation of 2NO₂ molecules on graphenylene-Pt surface more easily occur due to the rather lower energy barrier (<0.4 eV). Furthermore, the reaction pathways for NO and CO oxidations through TER mechanism on graphenylene-Pd sheet are further investigated and Table 4 shows their corresponding energy barriers. The formation of 2NO₂ molecules via TER mechanism have smaller E_{bar} (0.00 eV and 0.33 eV) than those of 2CO molecules (0.73 eV and 0.48 eV), which is similar as the same oxidation reactions on Pd doped graphene.^[57] This result illustrates that the interaction of 2NO and O₂ via TER mechanism is more easily to proceed. For the NO and CO oxidation reactions, the catalytic processes on graphenylene-Pd sheet have the relatively smaller energy barriers than those on graphenylene-Pt sheet, illustrating that the graphenylene-Pd sheet exhibits the high catalytic activity for LH and TER mechanisms.

2.3.4. NER Mechanism

Recent theoretical works have demonstrated a New ER (NER) mechanism,^[59] there are three molecules oxidation reactions involving one preadsorbed O₂ and two CO (or two NO) molecules probably through the pathway of O₂* + 2NO → OONNOO* → 2NO₂ or O₂* + 2CO → OOCOO* → 2CO₂. The NO

and CO oxidation reactions on graphenylene-Pt sheet through NER mechanism are shown in Figure 11. For the NO oxidation reactions, the NO molecules getting close to the preadsorbed O₂ and their distances gradually decrease from 2.49 Å to 1.24 Å. By overcoming the TS1 with an energy barrier of 0.18 eV, the MS configuration of OONNOO is dissociated and new two O–N–O connected by N–N anchored at the Pt atom. From the MS to FS, the MS configuration dissociates to form two NO₂ molecules without any energy barrier, as shown in Figure 11a. Compared with LH (0.34 eV) and TER (0.38 eV) mechanism, the NER reactions have relatively smaller energy barrier (0.18 eV) on graphenylene-Pt sheet.

As shown in Figure 11b, the same CO oxidation processes through NER reaction on graphenylene-Pt are further investigated. From the IS to MS, the formation of OOCOO complex need to overcome a larger energy barrier (0.81 eV) than that of the generation of OONNOO, where the formed new C–C bond and C–O bonds are 1.54 Å and 1.33 Å, respectively. Subsequently, the OOCOO complex dissociate to form two CO₂ molecules, which has a relatively smaller energy barrier (0.64 eV) than that of the formation process. However, the NER reactions for CO oxidation are still larger than those of the TER (0.74 eV), ER (0.27 eV) and LH (0.36 eV) mechanisms, indicating that the probability of NER reactions on graphenylene-Pt may not be high for CO oxidation.

In addition, the calculated energy barriers for NO and CO oxidations via NER mechanism on graphenylene-Pd sheet are displayed in Table 4. It is found that the formation of OONNOO (or OOCOO) complex have smaller energy barriers (0.14 eV and 0.07 eV) than that on the graphenylene-Pt, and the generation of 2NO₂ or 2CO₂ molecules are barrierless process. The small enough energy barriers for NO oxidation reactions on graphenylene-NM sheets indicate that the NER mechanism may be the more preferable reaction pathway, however, the weaker adsorption of O₂ compared with CO and NO illustrates that the preadsorbed O₂ is not favored. Hence, there is a low occurrence

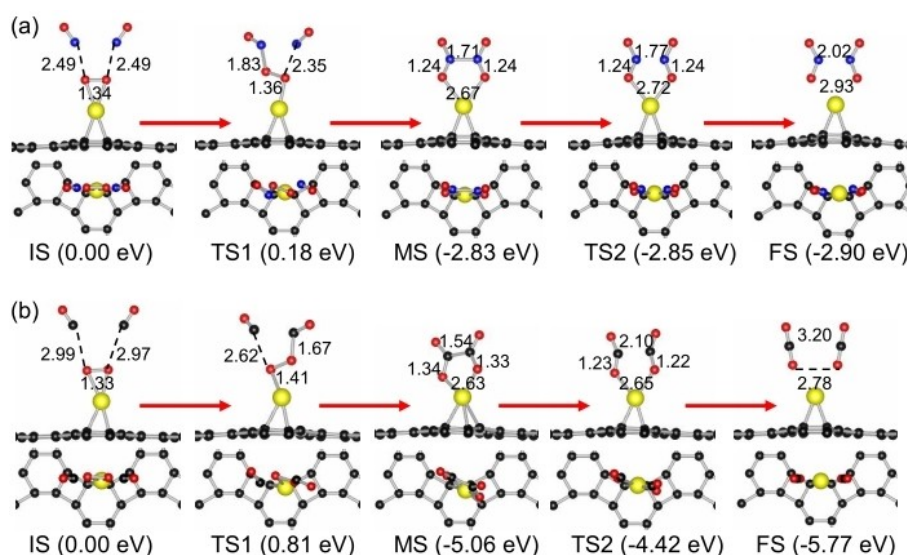


Figure 11. The reaction pathways for a) O₂–2NO and b) O₂–2CO through NER mechanism.

possibility for NER reaction pathways compared with other reaction mechanisms.

To conclude, the adsorption properties of gas reactants and catalytic reactions for NO and CO oxidation on different graphenylene-NM sheets are comparably investigated through LH, ER, TER and NER mechanisms. Firstly, the adsorbed NO and CO molecules are more stable than the O_2 molecule, and these isolated gases can regulate the electronic and magnetic properties of graphenylene-NM systems. Besides, the high stability of 2NO and 2CO easily occupy the active site of NM catalyst, and the coadsorption of 2NO molecules has relatively larger E_{ads} than that of 2CO. The adsorption reaction configurations as IS may determine the reaction pathways and energy barriers for NO and CO oxidations.^[60] The calculated E_{ads} represents the degree of interaction between gas species and supported catalysts, namely, the stability order for gas reactants is $2NO > 2CO > NO-O_2 > CO-O_2 > NO > CO > O_2$. Therefore, the preadsorbed 2NO and 2CO molecules as the IS reaction configuration through ER and TER mechanisms may act as a leading role in the first stage due to its high stability. Then, the coadsorption of $NO-O_2$ and $CO-O_2$ as the IS configuration for CO and NO oxidations may occur in the second stage through LH mechanisms. In comparison, there is a low occurrence possibility for the preadsorbed O_2 reacting with 2NO or 2CO molecules via NER mechanism, since the single O_2 has the lower adsorption energy compared with other reactant species.

Based on the adsorption stability and occurrence possibility for the gas reactant configurations, the more preferable reaction pathways for NO and CO oxidation are comparably analyzed. In the NO oxidation reactions, the catalytic processes through TER and LH mechanisms have close energy barriers (< 0.4 eV) on graphenylene-NM sheets. For graphenylene-Pt sheet, the formations of ONO-ONO and OONO complex are the rate-controlling steps in the oxidation of the first NO molecule with energy barriers (0.38 eV and 0.34 eV). Similar as graphenylene-Pt, the generated ONO-ONO and OONO complex also have close E_{bar} (0.33 eV and 0.31 eV) on graphenylene-Pd. For the CO oxidation reactions, the interactions between 2NO and 2CO via the ER reactions to generate the $2CO_2$ and N_2 molecules on graphenylene-Pt sheet. This reaction has the rather lower energy barriers (< 0.3 eV) than that on graphenylene-Pd sheet. Besides, the coadsorption of $CO-O_2$ molecules to product the OOCO complex as rate-controlling step with the smaller E_{bar} (0.36 eV and 0.33 eV) compared with the formation of OCO-OCO (0.74 eV and 0.73 eV), yet these energy barrier values are larger than those of the ER reactions. Although the NO oxidation reactions on graphenylene-NM through NER mechanism (< 0.2 eV) has much smaller energy barriers than the ER, LH and TER mechanisms, yet the relatively low stability of O_2 indicates that the probability of NER reaction pathways may not be high.

According to the calculated energy barriers on graphenylene-NM sheets, the CO oxidations reactions on graphenylene-NM through the ER mechanism ($2NO^* + 2CO \rightarrow N_2^* + 2CO_2$) is energetically more favorable reaction pathways than other mechanisms. The catalytic oxidation of NO on graphenylene-NM through TER mechanisms have relatively smaller energy

barriers (< 0.4 eV) than those of the CO oxidation. The NO and CO oxidation reactions via the LH mechanism have the close energy barriers, which is consistent with the distributions of d -band center of Pt and Pd catalysts anchored graphenylene. In all, the catalytic oxidation of CO via ER mechanism is more likely to happen than NO in the first stage, and the formed CO_2 is easily desorbed at room temperature. In the second stage, there are small energy barriers for the NO oxidation reactions through TER mechanism, yet the releasing NO_2 product is rather rate-determining. Meanwhile, the CO and NO oxidation reactions via the LH mechanism exhibit the higher occurrence possibility than those of the NER mechanism due to the coadsorbed gas molecules exhibit the relatively high stability. Therefore, there are different occurrence possibility for NO and CO oxidations via four reaction mechanisms on graphenylene-NM sheets.

2.3.5. Effects of Temperature and Entropy

Among these oxidation reactions, the CO oxidations reactions on graphenylene-Pt through ER mechanism ($2NO^* + 2CO \rightarrow N_2^* + 2CO_2$) is energetically more favorable, and the temperature (T) and entropy (S) affect the CO oxidation reactions via ER mechanism, as well as the corresponding change in Gibbs free energy (ΔG) and $T\Delta S$ values are investigated. In thermodynamics, ΔG is defined as $\Delta G = \Delta E + \Delta E_{ZPE} - T\Delta S$, where ΔE represents the change in total energy of the reaction at 0 K, and ΔE_{ZPE} is the change in zero point vibration energy. ΔS is the change in entropy, defined as $\Delta S = \Delta S_{trans} + \Delta S_{rot} + \Delta S_{vib}$ where ΔS_{trans} , ΔS_{rot} and ΔS_{vib} denotes the contributions of translation, rotation and vibration modes, respectively.

Table 5 shows that the ΔG and $T\Delta S$ values for the CO oxidation via ER reaction steps. As evident, a distinct behavior is found for the variation of $T\Delta S$ values of these reaction steps with the increase of T. It is found that $T\Delta S$ decreases (becomes more negative) for the IS \rightarrow MS, when the temperature varies from 200 to 600 K, which is in agreement with the trend for the MS \rightarrow FS. Moreover, ΔG values for these reaction steps are negative and increases with an increase in the temperature. It is note that the total ΔG values for the whole CO oxidation reactions (IS \rightarrow FS) are all negative, indicating that the CO oxidation via the ER mechanism is a thermodynamically favorable process at certain temperatures.

3. Conclusions

In this work, the adsorption configurations of different reactant species on single-atom Pt and Pd anchored graphenylene substrates are investigated using DFT methods, as well as these adsorbed gases can regulate the electronic and magnetic properties of systems. According to the calculated adsorption energies, the single NO and CO or 2NO and 2CO molecules are more stable than that of the O_2 or $NO-O_2$ and $CO-O_2$ molecules. Hence, the reaction occurrence possibility for the ER and TER mechanism are more than those of the LH and NER mechanisms. For the TER mechanism, the catalytic oxidations of

Table 5. Calculated Gibbs free energy change (ΔG , in eV) and $T\Delta S$ (in eV) values for different steps in the CO oxidation reaction via the ER mechanism.

T [K]	IS→MS ΔG	$T\Delta S$	MS→FS ΔG	$T\Delta S$	IS→FS ΔG	$T\Delta S$
no correction	−0.32	−	−0.42	−	−0.74	−
100	−0.31	−0.02	−0.41	−0.02	−0.72	−0.04
200	−0.28	−0.08	−0.39	−0.04	−0.67	−0.12
250	−0.26	−0.11	−0.38	−0.06	−0.64	−0.17
298	−0.23	−0.14	−0.37	−0.08	−0.60	−0.22
350	−0.21	−0.18	−0.35	−0.10	−0.56	−0.28
400	−0.18	−0.21	−0.34	−0.11	−0.52	−0.33
500	−0.13	−0.28	−0.31	−0.15	−0.44	−0.43
600	−0.07	−0.35	−0.28	−0.18	−0.35	−0.54

NO molecules have the smaller energy barriers than those of the CO oxidation. Among these oxidation pathways, the interaction between 2NO and 2CO via the ER mechanism to generate 2CO₂ and N₂ products is an energetically favorable reaction on graphenylene-Pt sheet (<0.3 eV), and the calculated negative ΔG values illustrate that the ER mechanism for CO oxidation is a thermodynamically possible process. Therefore, the high occurrence possibility for NO and CO oxidation processes have small energy barriers via different reaction mechanisms, indicating that the graphenylene-NM are potential efficient and high activity catalysts to remove toxic molecules.

Acknowledgments

This work was supported by the National Natural Science Foundation of China (Grant Nos. 61674053, 11904328 and 62074053), Science & Technology Innovation Talents in Universities of Henan Province (Grant No. 18HASTIT030), the key Young Teachers of Henan Province (Grant No. 2017GGJS179), the Key Scientific Research Project of Henan College (Grant Nos. 20A140030, 21A140029), the Key Technologies Research and Development Program of Henan Province (Grant Nos. 202102210201, 212102210486). Aid program for Science and Technology Innovative Research Team and Open Research Fund of Zhengzhou Normal University.

Conflict of Interest

The authors declare no conflict of interest.

Keywords: density functional theory • graphene-like material • NO and CO oxidation • single-atom catalyst • reaction mechanisms

- [1] S. Ji, Y. Chen, X. Wang, Z. Zhang, D. Wang, Y. Li, *Chem. Rev.* **2020**, *120*, 11900–11955.
- [2] X. Li, X. Yang, Y. Huang, T. Zhang, B. Liu, *Adv. Mater.* **2019**, *31*, 1902031.
- [3] C. Chang, C. Cheng, C. Wei, *J. Chem. Phys.* **2008**, *128*, 124710.
- [4] X. Liu, M.-H. Liu, Y.-C. Luo, C.-Y. Mou, S. D. Lin, H. Cheng, J.-M. Chen, J.-F. Lee, T.-S. Lin, *J. Am. Chem. Soc.* **2012**, *134*, 10251–10258.
- [5] S. N. Rashkeev, A. R. Lupini, S. H. Overbury, S. J. Pennycook, S. T. Pantelides, *Phys. Rev. B* **2007**, *76*, 035438.
- [6] X. Q. Gong, Z. P. Liu, R. Raval, P. Hu, *J. Am. Chem. Soc.* **2004**, *126*, 8–9.
- [7] V. Shapovalov, H. Metiu, *J. Catal.* **2007**, *245*, 205–214.
- [8] L. Liu, F. Zhou, L. Wang, X. Qi, F. Shi, Y. Deng, *J. Catal.* **2010**, *274*, 1–10.
- [9] H. J. Freund, G. Meijer, M. Scheffler, R. Schlogl, M. Wolf, *Angew. Chem. Int. Ed.* **2011**, *50*, 10064–10094; *Angew. Chem.* **2011**, *123*, 10242–10275.
- [10] Z. W. Chen, J. M. Yan, W. T. Zheng, Q. Jiang, *Sci. Rep.* **2015**, *5*, 11230.
- [11] E. Yoo, T. Okada, T. Akita, M. Kohyama, I. Honma, J. Nakamura, *J. Power Sources* **2011**, *196*, 110–115.
- [12] I. Fampiou, A. Ramasubramaniam, *J. Phys. Chem. C* **2013**, *117*, 19927–19933.
- [13] N. Cuong, A. Sugiyama, A. Fujiwara, T. Mitani, D. Chi, *Phys. Rev. B* **2009**, *79*, 235417.
- [14] I. Fampiou, A. Ramasubramaniam, *J. Phys. Chem. C* **2015**, *119*, 8703–8710.
- [15] B. Qiao, A. Wang, X. Yang, L. F. Allard, Z. Jiang, Y. Cui, J. Liu, J. Li, T. Zhang, *Nat. Chem.* **2011**, *3*, 634–641.
- [16] A. Wang, J. Li, T. Zhang, *Nat. Chem. Rev.* **2018**, *2*, 65–81.
- [17] A. Geim, K. Novoselov, *Nat. Mater.* **2007**, *6*, 183–191.
- [18] K. M. Yam, N. Guo, Z. Jiang, S. Li, C. Zhang, *Catalysts* **2020**, *10*, 53.
- [19] L.-H. Zhang, Y. Shi, Y. Wang, N. R. Shiju, *Adv. Sci.* **2020**, 1902126.
- [20] W. Yang, Z. Gao, X. Liu, C. Ma, X. Ding, W. Yan, *Fuel* **2019**, *243*, 262–270.
- [21] W. Yang, S. Xu, K. Ma, C. Wu, I. D. Gates, X. Ding, W. Meng, Z. Gao, *Nano Mater. Sci.* **2020**, *2*, 120–131.
- [22] Q. Song, B. Wang, K. Deng, X. Feng, M. Wagner, J. D. Gale, K. Müllen, L. Zhi, *J. Mater. Chem. C* **2013**, *1*, 38–41.
- [23] T. Hussain, M. Hankel, D. J. Searles, *J. Phys. Chem. C* **2017**, *121*, 14393–14400.
- [24] M. Hankel, D. J. Searles, *Phys. Chem. Chem. Phys.* **2016**, *18*, 14205–14215.
- [25] L. Wang, F. Li, J. Wang, Y. Li, W. Li, Y. Yang, M. Zhao, Y. Qu, *Phys. Chem. Chem. Phys.* **2020**, *22*, 9789–9795.
- [26] C. Xie, Z. Niu, D. Kim, M. Li, P. Yang, *Chem. Rev.* **2020**, *120*, 1184–1249.
- [27] S. S. Mulla, N. Chen, L. Cumarantunge, G. E. Blau, D. Y. Zemlyanov, W. N. Delgass, W. S. Epling, F. H. Ribeiro, *J. Catal.* **2006**, *241*, 389–399.
- [28] Z. Wang, F. Lin, S. Jiang, K. Qiu, M. Kuang, R. Whiddon, K. Cen, *Fuel* **2016**, *166*, 352–360.
- [29] H.-F. Wang, Y.-L. Guo, G. Lu, P. Hu, *J. Phys. Chem. C* **2009**, *113*, 18746–18752.
- [30] C. K. Narula, L. F. Allard, G. M. Stocks, M. Moses-DeBusk, *Sci. Rep.* **2014**, *4*, 7238.
- [31] T. Kropp, M. Mavrikakis, *ACS Catal.* **2019**, *9*, 6864–6868.
- [32] E. Fernández, L. Liu, M. Boronat, R. Arenal, P. Concepcion, A. Corma, *ACS Catal.* **2019**, *9*, 11530–11541.
- [33] F. Li, Y. Li, X. C. Zeng, Z. Chen, *ACS Catal.* **2015**, *5*, 544–552.
- [34] G. Kresse, J. Furthmüller, *Comput. Mater. Sci.* **1996**, *6*, 15–50.
- [35] G. Kresse, J. Furthmüller, *Phys. Rev. B* **1996**, *54*, 11169–11186.
- [36] J. Perdew, K. Burke, M. Ernzerhof, *Phys. Rev. Lett.* **1996**, *77*, 3865–3868.
- [37] G. Kresse, D. Joubert, *Phys. Rev. B* **1999**, *59*, 1758–1775.
- [38] G. Henkelman, A. Arnaldsson, H. Jónsson, *Comput. Mater. Sci.* **2006**, *36*, 354–360.
- [39] G. Henkelman, B. Uberuaga, H. Jónsson, *J. Chem. Phys.* **2000**, *113*, 9901–9904.
- [40] G. Henkelman, H. Jónsson, *J. Chem. Phys.* **2000**, *113*, 9978–9985.
- [41] T. Zhu, J. Li, S. Yip, *Phys. Rev. Lett.* **2004**, *93*, 25503.
- [42] Y. N. Tang, Z. X. Yang, X. Q. Dai, *J. Chem. Phys.* **2011**, *135*, 224704.
- [43] Y. Tang, Z. Yang, X. Dai, *Phys. Chem. Chem. Phys.* **2012**, *14*, 16566–16572.
- [44] V. Zolyomi, A. Ruzsnyak, J. Kurti, C. J. Lambert, *J. Phys. Chem. C* **2010**, *114*, 18548–18552.
- [45] Y. Tang, Z. Yang, X. Dai, *J. Nanopart. Res.* **2012**, *14*, 844.

- [46] H. Liu, B. Wang, M. Fan, N. Henson, Y. Zhang, B. F. Towler, H. G. Harris, *Fuel* **2013**, *113*, 712–718.
- [47] W. Yang, Z. Gao, X. Liu, X. Li, X. Ding, W. Yan, *Catal. Sci. Technol.* **2018**, *8*, 4159–4168.
- [48] Y. Tang, J. Zhou, W. Chen, H. Chai, Y. Li, Z. Feng, X. Dai, *J. Mol. Catal.* **2019**, *476*, 110524.
- [49] Z. Lu, P. Lv, Z. Yang, S. Li, D. Ma, R. Wu, *Phys. Chem. Chem. Phys.* **2017**, *19*, 16795–16805.
- [50] Z. Lu, P. Lv, J. Xue, H. Wang, Y. Wang, Y. Huang, C. He, D. Ma, Z. Yang, *RSC Adv.* **2015**, *5*, 84381–84388.
- [51] Y. Tang, W. Chen, J. Zhou, H. Chai, Y. Li, Y. Cui, Z. Feng, X. Dai, *Fuel* **2019**, *253*, 1531–1544.
- [52] Z. Lu, M. Yang, D. Ma, P. Lv, S. Li, Z. Yang, *Appl. Surf. Sci.* **2017**, *426*, 1232–1240.
- [53] Y. Tang, W. Chen, H. Zhang, Z. Wang, D. Teng, Y. Cui, Z. Feng, X. Dai, *Phys. Chem. Chem. Phys.* **2020**, *22*, 16224–16235.
- [54] W. Chen, Z. Wang, Y. Cui, Z. Li, Y. Li, X. Dai, Y. Tang, *New J. Chem.* **2020**, *44*, 15733–15741.
- [55] E. H. Song, Z. Wen, Q. Jiang, *J. Phys. Chem. C* **2011**, *115*, 3678–3683.
- [56] L. Xin, S. Yanhui, D. Ting, M. Changong, H. Yu, *Phys. Chem. Chem. Phys.* **2014**, *16*, 23584–23593.
- [57] G. Xu, R. Wang, F. Yang, D. Ma, Z. Yang, Z. Lu, *Carbon* **2017**, *118*, 35–42.
- [58] H. Zhang, S. Fang, Y. H. Hu, *Catal. Rev.* **2020**, 1–42.
- [59] G. Xu, R. Wang, Y. Ding, Z. Lu, D. Ma, Z. Yang, *J. Phys. Chem. C* **2018**, *122*, 23481–23492.
- [60] Y. Tang, H. Zhang, W. Chen, Z. Li, Z. Liu, D. Teng, X. Dai, *Appl. Surf. Sci.* **2020**, *508*, 145245.

Manuscript received: December 15, 2020
Revised manuscript received: February 10, 2021
Accepted manuscript online: February 18, 2021
Version of record online: February 25, 2021